Fluid Phase Equilibria 313 (2012) 32–37

Contents lists available at SciVerse ScienceDirect

Fluid Phase Equilibria

journal homepage: www.elsevier.com/locate/fluid

High pressure phase equilibria in methane + waxy systems. 3. Methane + a synthetic distribution of paraffin ranging from n-C_{13} to n-C_{22}

Jérôme Pauly[a], João A.P. Coutinho[b], Jean-Luc Daridon[a,*]

[a] Laboratoire des Fluides Complexes, Université de Pau, BP 1155, 64013 Pau Cedex, France
[b] CICECO, Departamento de Quimica da Universidade de Aveiro, 3810-193 Aveiro, Portugal

ARTICLE INFO

Article history:
Received 8 July 2011
Received in revised form 2 September 2011
Accepted 7 September 2011
Available online 5 October 2011

Keywords:
Solid–liquid equilibrium
Wax
Paraffin

ABSTRACT

Liquid–vapor and fluid–waxy solid phase transitions were measured under pressure on a pseudo binary system made up of methane + a waxy distribution of normal paraffins ranging from C_{13} to C_{22}. The composition of the paraffins in the waxy fraction was defined in order to obtain an average molecular weight equal to that of pure heptadecane. Measurements were carried out up to 90 MPa by using a synthetic method on various mixtures ranging from 0 to 99% of methane. Results were compared to the phase equilibrium data of the binary system methane + heptadecane in the same conditions.

1. Introduction

Changes in pressure and temperature during oil and gas production operations can lead to heavy organic separation from reservoir fluids. In particular, the presence of heavy paraffins in reservoir fluids can produce the formation of waxy solid deposits when their temperatures drop from reservoir to ambient temperature or due to loss of light end by depressurization, even in fluids containing low concentrations of high molecular weight components [1,2]. Accumulation of wax in production facilities as well as in transportation pipelines is a source of expensive problems. The remediation of solid deposits being very costly, it is crucial to evaluate the risk of wax formation and to be able to predict where wax may appear and accumulate. In order to evaluate the potential risks of wax precipitation it is very important to correctly know the liquid–solid phase transitions as well as the vapour–solid phase equilibrium. Some gas condensates may contain very high molecular weight paraffin that may precipitate during depressurization [3,4]. Although the wax content is usually low in such fluids, it may lead to huge damage in surface facilities and in particular in subsea transportation lines. The effect of depressurization on wax precipitation does not arise from the pressure change itself [5–7] but mainly from the change of composition caused by the phase transition occurring during gas production. The influence of high gas content is usually not correctly represented by thermodynamic models that must be improved in order to make possible the prediction of live oil behaviour from wax appearance temperature measurements carried out on stock tank oils at atmospheric pressure. To improve the description of wax precipitation in gas condensates, accurate liquid–solid phase equilibrium data of systems covering a wide range of gas composition are required. With this goal in mind, Flöter et al. [8–13] and Machado et al. [14] studied extensively the phase diagrams of highly dissymmetric binary systems methane plus one heavy paraffin. Furthermore, Machado et al. [15] studied solid precipitation in a model system made of methane + two paraffins.

In order to extend the available data of this type to long paraffin distribution systems, we have started a programme of fluid–solid phase equilibrium measurements on dissymmetric mixtures made up of a gas and a heavy paraffin distribution. This paper, which follows the works on the binary mixture methane + n-heptadecane [16], and on the methane + (n-hexadecane + n-heptadecane + n-octadecane) system [17], focuses on the pseudo binary made up of a methane + a mixture of ten paraffins ranging from n-C_{13} to n-C_{22}. To compare the phase equilibrium data of these three systems and in particular to study the influence of the paraffin distribution length, the composition of the paraffin inside the heavy fraction of pseudo binary systems was defined with a regular decrease, as observed in real oils, but with an average molecular weight of 240.5 g mol^{-1} that corresponds to the molecular weight of pure heptadecane.

2. Experimental

Measurements of both fluid phase equilibria and fluid–solid phase transitions were carried out by a synthetic method that does not have the need to sample and analyse the phases in equilibrium

* Corresponding author.
E-mail address: jean-luc.daridon@univ-pau.fr (J.-L. Daridon).

0378-3812/$ – see front matter © 2011 Elsevier B.V. All rights reserved.
doi:10.1016/j.fluid.2011.09.008

[18]. The apparatus, which has been described in a previous paper [16], is essentially made up of a full visibility PVT cell. It consists in a variable-volume vessel closed at one end by a sapphire window. A video acquisition system, made up of an endoscope plus a video camera, is placed right in front of the sapphire window and connected to a screen for observation of the phase transitions occurring inside the cell. It is arranged to work up to 100 MPa and in a temperature ranging from 243.15 K to 393.15 K. The pressure is measured by a piezoresistive silicon pressure transducer (Kulite) placed inside the cell in order to minimize dead volume. The temperature is regulated by circulating a heat-carrier fluid through flow lines managed inside the pump body. The temperature is measured with a calibrated platinum resistance inserted inside the cell and connected to a high-precision thermometer (AOIP).

This high pressure cell was designed to minimize the dead volume in order to enable an easy preparation of gas–liquid mixtures directly in the interior of the measurement cell. The waxy fraction composed of several n-paraffins was previously prepared by weighing in an auxiliary tank. It was then introduced into the measurement cell in liquid phase and the amount of the heavy fraction transferred to the cell is determined by weighing the auxiliary tank with an accuracy of ±0.1 mg. Finally, the gas is added under pressure from an aluminium reservoir tank connected to the measuring cell by means of a flexible high pressure capillary and put on a high weight/high precision balance with an accuracy of ±1 mg. The mass of gas added into the cell is obtained by weighing the gas tank during filling. The phase boundary of a mixture of known composition is then measured by observing visually the phase disappearance by changing either the pressure or temperature conditions. According to the shape of the curves, bubble conditions were determined by observing the disappearance pressure of the last bubble during an isothermal process whereas solid disappearance conditions were mostly determined by measuring the wax disappearance temperature (WDT) at fixed pressure. During both processes, conditions are changed stepwise and the mixture is continuously stirred thanks to a magnetic bar placed inside the cell in order to keep the system close to equilibrium during all the experiments. The boundaries between the three phase L + V + S and the two phase L + V domains were experimentally determined by measuring the disappearance conditions of the last solids and the end of this boundary curve was indirectly deduced by recording the intersection of the bubble (or dew) curve with fluid–solid transition line. Using this technique, wax disappearance temperatures are repeatable to within ±0.2 K whereas reproducibility of bubble or dew pressure is within ±0.05 MPa in such kind of mixture. The liquid–solid transitions of the sole waxy fraction cannot be accurately measured in the PVT cell as the minimum sample needed in this cell is too large. It was determined up to 100 MPa by microscopy as reported in a previous work [19].

The paraffins used in the waxy fraction were supplied by Fluka or Sigma. No further treatments were carried out. The purity given by these chemical companies for each compound is listed in Table 1. The methane was supplied by Messer with a guaranteed purity of 99.995 vol%.

3. Results and discussion

The waxy fraction used in the studied mixtures was composed by a distribution of ten consecutive paraffins ranging from n-C_{13} to n-C_{22} with a molar mass composition regularly decreasing according to recurrence relationship:

$$Xc_{n+1} = \alpha Xc_n$$

with a coefficient α defined to have the average molecular weight of the waxy part similar to that of pure heptadecane (240.5 g mol^{-1}).

Table 1
Waxy fraction composition.

	Wax_1	Wax_2	Wax_3	Supplier	Purity (mol%)
n-C_{13}	12.98%	12.95%	13.12%	Fluka	>99.0
n-C_{14}	12.12%	12.39%	12.08%	Fluka	>99.0
n-C_{15}	11.38%	11.35%	11.38%	Fluka	>99.0
n-C_{16}	10.72%	10.62%	10.59%	Fluka	>99.8
n-C_{17}	10.01%	10.06%	9.97%	Fluka	99.0
n-C_{18}	9.44%	9.41%	9.45%	Aldrich	99.0
n-C_{19}	8.99%	8.92%	8.95%	Aldrich	99.0
n-C_{20}	8.50%	8.48%	8.52%	Aldrich	99.0
n-C_{21}	8.12%	8.08%	8.15%	Fluka	>98.0
n-C_{22}	7.75%	7.73%	7.79%	Aldrich	99.0
Mw (g mol^{-1})	240.80	240.67	240.81		
α	0.942	0.943	0.940		

Actually, due to the number of experiments carried out, 3 waxy fractions, called wax_1, wax_2, and wax_3 had to be prepared with an overall composition closely related but not completely identical. The exact composition of each waxy fraction used is listed in Table 1 along with the value of the α parameter and its average molecular weight.

The wax disappearance temperatures of the heavy fraction are plotted as a function of pressure in Fig. 1 along with the melting temperature of the pure n-C_{17} [16]. The WDT measured in the ternary mixture n-C_{16} + n-C_{17} + n-C_{18} [17], with the same average molecular weight, is also shown in this figure. It can be observed that the WDT of the heavy fraction is similar to the melting temperature of n-heptadecane. A positive difference of only 1 K is observed at atmospheric pressure whereas there is a negative difference of 1.5 K from the ternary mixture. Moreover the average slope of the WDT versus pressure between 0.1 and 80 MPa is decreasing as the paraffin distribution is enlarged. Its value is of 0.195 K MPa^{-1} for the paraffin distribution here studied whereas it reaches 0.215 K MPa^{-1} for n-heptadecane. This slope change reveals the existence of an excess volume that increases as the distribution complexity increases. This effect must be taken into consideration while modelling the wax appearance temperature in reservoir fluid under pressure [20–22].

Isoplethic measurements were carried out on several mixtures with methane content ranging from 0 to 99 mol%. The results are listed in Table 2 along with the nature of the transitions observed. Isopleths on *P*–*T* diagrams of mixtures exhibiting bubble points (with methane content less than 90%) are displayed in Fig. 2. It can be seen that the WDT curves appear to be parallel and independent

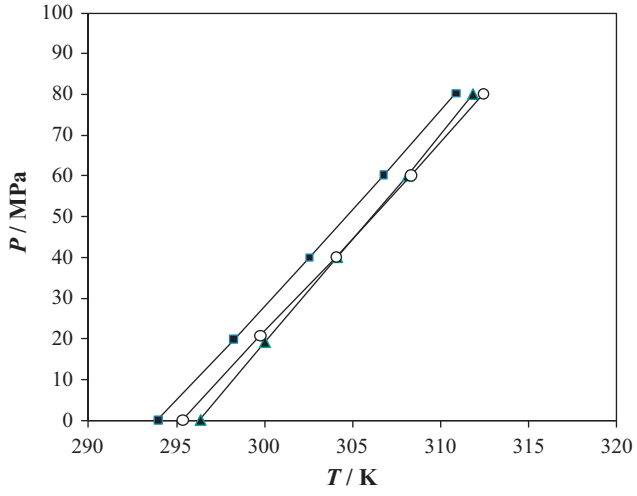

Fig. 1. Wax disappearance temperature as a function of pressure for the waxy fraction. ▲: waxy fraction; ■: n-C_{16} + n-C_{17} + n-C_{18} [17]; ○: pure heptadecane [16].

Table 2
Liquid–vapor[a] and fluid–solid phase transitions[b] at a given overall composition (in mol%) of the pseudo binary system methane + waxy fraction.

T (K)	P (MPa)		T (K)	P (MPa)		T (K)	P (MPa)	
0% of CH_4 + 100% of wax_1								
296.35	0.1	L+S→L	300.0	19.2	L+S→L	304.1	40	L+S→L
308.1	60	L+S→L	311.8	80	L+S→L			L+S→L
6.34% of CH_4 + 93.66% of wax_1								
295.55	1.31	L+V→L	313.05	1.25	L+V→L	332.95	1.17	L+V→L
343.00	1.13	L+V→L	353.15	1.10	L+V→L	373.00	1.01	L+V→L
296.10	0.10	L+V+S→L+V	296.00	0.24	L+V+S→L+V	295.80	0.54	L+V+S→L+V
295.70	0.84	L+V+S→L+V	295.60	1.14	L+V+S→L+V	295.55	1.31	Crossover
295.60	1.44	L+S→L	295.70	1.93	L+S→L	297.20	9.88	L+S→L
300.90	29.72	L+S→L	304.70	49.54	L+S→L	308.40	69.35	L+S→L
312.00	89.14	L+S→L						
19.24% of CH_4 + 80.76% of wax_1								
294.45	4.33	L+V→L	297.65	4.40	L+V→L	307.95	4.51	L+V→L
313.15	4.62	L+V→L	322.65	4.83	L+V→L	333.05	5.00	L+V→L
343.15	5.21	L+V→L	352.55	5.36	L+V→L	362.15	5.43	L+V→L
372.35	5.54	L+V→L	295.95	0.95	L+V+S→L+V	295.45	2.06	L+V+S→L+V
295.05	2.93	L+V+S→L+V	294.65	3.93	L+V+S→L+V	294.55	4.33	Crossover
294.85	5.42	L+S→L	295.65	9.89	L+S→L	297.85	19.83	L+S→L
299.95	29.74	L+S→L	303.95	49.66	L+S→L	307.65	69.34	L+S→L
311.25	89.17	L+S→L						
32.19% of CH_4 + 67.81% of wax_1								
292.95	8.11	L+V→L	294.15	8.22	L+V→L	305.05	8.70	L+V→L
312.15	8.98	L+V→L	323.45	9.37	L+V→L	333.15	9.67	L+V→L
342.55	10.03	L+V→L	352.45	10.45	L+V→L	362.15	10.77	L+V→L
371.95	11.06	L+V→L	295.25	1.54	L+V+S→L+V	294.95	2.37	L+V+S→L+V
294.35	3.93	L+V+S→L+V	293.70	5.89	L+V+S→L+V	292.95	7.91	L+V+S→L+V
292.95	8.11	Crossover	297.05	29.85	L+S→L	301.05	49.62	L+S→L
304.95	69.45	L+S→L	308.45	89.27	L+S→L			
41.30% of CH_4 + 58.70% of wax_1								
291.85	13.00	L+V→L	292.95	13.03	L+V→L	303.65	13.38	L+V→L
309.65	13.71	L+V→L	323.25	14.06	L+V→L	338.45	14.34	L+V→L
353.05	14.68	L+V→L	363.15	14.92	L+V→L	373.15	15.15	L+V→L
295.25	2.43	L+V+S→L+V	294.25	4.83	L+V+S→L+V	293.15	7.24	L+V+S→L+V
292.35	9.85	L+V+S→L+V	291.75	13.00	Crossover	292.25	14.94	L+S→L
293.25	19.73	L+S→L	295.25	29.82	L+S→L	299.05	49.55	L+S→L
302.65	69.63	L+S→L	306.40	89.39	L+S→L			
49.72% of CH_4 + 50.28% of wax_1								
290.85	16.96	L+V→L	303.15	19.08	L+V→L	305.15	19.12	L+V→L
324.15	19.58	L+V→L	333.15	19.91	L+V→L	342.75	20.15	L+V→L
363.15	20.51	L+V→L	295.15	2.88	L+V+S→L+V	294.05	5.23	L+V+S→L+V
293.15	7.47	L+V+S→L+V	292.45	9.75	L+V+S→L+V	291.25	13.96	L+V+S→L+V
290.85	16.96	Crossover	291.15	18.95	L+S→L	291.45	20.09	L+S→L
295.35	40.89	L+V+S→L+V	296.95	49.74	L+S→L	300.75	69.99	L+S→L
59.74% of CH_4 + 40.26% of wax_1								
290.35	27.68	L+V→L	299.75	27.65	L+V→L	312.75	27.57	L+V→L
331.15	27.43	L+V→L	342.15	27.33	L+V→L	362.15	27.16	L+V→L
372.15	27.04	L+V→L	294.15	4.86	L+V+S→L+V	292.25	9.88	L+V+S→L+V
291.35	14.86	L+S→L	290.55	19.97	L+V+S→L+V	290.15	24.97	L+S→L
289.95	27.68	Crossover	290.55	30.06	L+S→L	294.35	49.90	L+S→L
297.95	70.08	L+S→L	301.55	89.74	L+S→L			
69.95% of CH_4 + 30.05% of wax_2								
290.15	39.62	L+V→L	298.35	39.28	L+V→L	309.95	38.89	L+V→L
323.15	38.45	L+V→L	331.85	38.08	L+V→L	351.15	37.38	L+V→L
372.15	36.32	L+V→L	292.15	9.95	L+V+S→L+V	290.55	16.97	L+V+S→L+V
289.75	24.98	L+V+S→L+V	289.55	30.09	L+V+S→L+V	289.65	37.49	Crossover
293.65	59.82	L+S→L	297.15	79.71	L+S→L	300.45	98.59	L+S→L
79.73% of CH_4 + 20.27% of wax_2								
291.35	60.05	L+V→L	305.85	56.87	L+V→L	314.85	55.31	L+V→L
323.15	53.98	L+V→L	332.85	52.87	L+V→L	344.85	51.59	L+V→L
352.75	50.77	L+V→L	363.25	49.77	L+V→L	372.25	49.11	L+V→L
292.05	9.95	L+V+S→L+V	290.35	19.97	L+V+S→L+V	289.65	30.12	L+V+S→L+V
289.95	40.08	L+V+S→L+V	290.45	50.07	L+V+S→L+V	291.15	60.05	Crossover
293.05	69.98	L+S→L	294.45	79.41	L+S→L	295.95	89.81	L+S→L
89.76% of CH_4 + 10.24% of wax_2								
298.85	73.85	L+V→L	308.65	71.23	L+V→L	308.85	71.13	L+V→L
318.25	68.96	L+V→L	328.15	66.97	L+V→L	337.75	65.32	L+V→L
347.45	63.80	L+V→L	357.35	62.35	L+V→L	372.95	60.24	L+V→L
290.25	20.17	L+V+S→L+V	290.05	40.07	L+V+S→L+V	291.35	59.95	L+V+S→L+V
293.15	75.68	Crossover	293.55	79.85	L+S→L	294.05	84.84	L+S→L
294.45	89.84	L+S→L						
92.82% of CH_4 + 7.18% of wax_3								
303.95	74.77	L+V→L	313.65	72.17	L+V→L	322.95	70.02	L+V→L
333.15	67.89	L+V→L	342.85	66.03	L+V→L	352.95	64.38	L+V→L
362.25	63.04	L+V→L	373.15	61.70	L+V→L			

Table 2 (*Continued*)

T (K)	*P* (MPa)		*T* (K)	*P* (MPa)		*T* (K)	*P* (MPa)	
93.48% of CH_4 + 6.52% of wax_3								
303.15	75.10	L + V → L	313.85	72.11	L + V → L	323.65	69.89	L + V → L
333.35	67.93	L + V → L	343.15	66.18	L + V → L	353.05	64.53	L + V → L
362.55	63.59	L + V → L						
95.11% of CH_4 + 4.89% of wax_3								
302.55	75.75	L + V → V	312.85	73.00	L + V → V	323.55	70.52	L + V → V
333.85	68.28	L + V → V	343.65	66.27	L + V → V	353.95	64.63	L + V → V
362.75	63.11	L + V → V						
95.96% of CH_4 + 4.04% of wax_3								
294.35	77.92	L + V → V	303.15	75.40	L + V → V	313.95	72.46	L + V → V
323.45	70.31	L + V → V	332.85	68.39	L + V → V	342.75	66.45	L + V → V
353.15	64.62	L + V → V	363.15	63.02	L + V → V	373.05	61.55	L + V → V
290.45	19.97	L + V + S → L + V	290.45	40.96	L + V + S → L + V	291.25	50.14	L + V + S → L + V
292.25	59.98	L + V + S → L + V	293.25	69.94	L + V + S → L + V	293.65	75.24	L + V + S → L + V
294.35	77.92	Crossover	294.90	84.00	V + S → V			
97.95% of CH_4 + 2.05% of wax_3								
303.15	68.81	L + V → V	313.95	66.95	L + V → V	323.25	65.76	L + V → V
332.25	63.96	L + V → V	343.65	61.65	L + V → V	353.15	60.10	L + V → V
362.15	58.57	L + V → V	290.45	20.07	L + V + S → L + V	289.95	30.08	L + V + S → L + V
291.05	40.00	L + V + S → L + V	292.35	50.00	L + V + S → L + V	293.95	59.88	L + V + S → L + V
295.35	69.75	Crossover	295.75	74.46	V + S → V			
99.08% of CH_4 + 0.92% of wax_3								
296.45	55.74	L + V → V	313.05	54.56	L + V → V	323.95	53.57	L + V → V
335.15	52.16	L + V → V	343.25	51.27	L + V → V	352.75	50.08	L + V → V
363.15	48.75	L + V → V	290.65	30.06	L + V + S → L + V	293.35	39.94	L + V + S → L + V
295.05	49.81	L + V + S → L + V	296.45	55.74	Crossover	295.15	67.28	V + S → V
294.15	72.82	V + S → V	293.45	79.87	V + S → V			

[a] Bubble or dew pressure uncertainty is 0.05 MPa.
[b] Solid disappearance temperature uncertainty is 0.2 K.

of the methane content in this composition range. The phase boundary between L–V and L–V–S seems to be superimposed up to 30 MPa. Beyond this pressure the curves of higher compositions slightly break away. This behaviour results from the system not being a real binary mixture and consequently the three phase equilibrium not being monovariant. It corresponds to a narrow zone in the *P*–*T* diagram.

The phase boundary between the three phase (L + V + S) and the two phase (L + V) equilibrium regions was measured by determining the wax disappearance conditions in the two fluid phase equilibrium system. The end of this phase boundary corresponds to the crossover of the bubble point curves and the WDT lines. For higher methane content, these curves present a minimum in temperature at around 40 MPa. The presence of such minimum was observed in binary systems made up of methane and one heavy paraffin [23,24]. It implies that wax can precipitate during decompression on an isothermal process. This retrograde phenomenon appears for temperatures ranging from the WDT at atmospheric pressure and the minimum temperature.

Measurements performed on mixtures having methane content higher than 96 mol% present a dew point curve in the investigated temperature range. The isopleths of these mixtures are presented in Fig. 3. In this composition range, the slope of WDT as a function of pressure changes with methane content. It decreases as the methane concentration increases. It even becomes negative

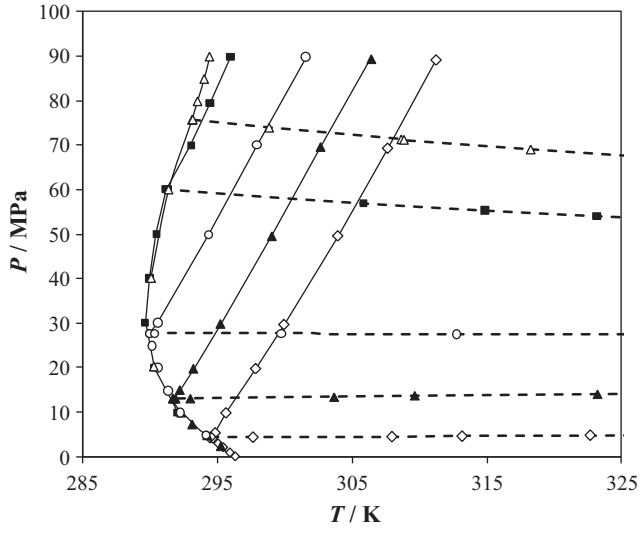

Fig. 2. *P*–*T* phase diagram of the system methane + waxy fraction for overall compositions (in mol% of CH_4) lower than 90%. Full line: wax disappearance temperatures; dotted line: bubble pressures. ◊: 20% of methane; ▲: 40% of methane; ◯: 60% of methane; ■: 80% of methane; △: 90% of methane.

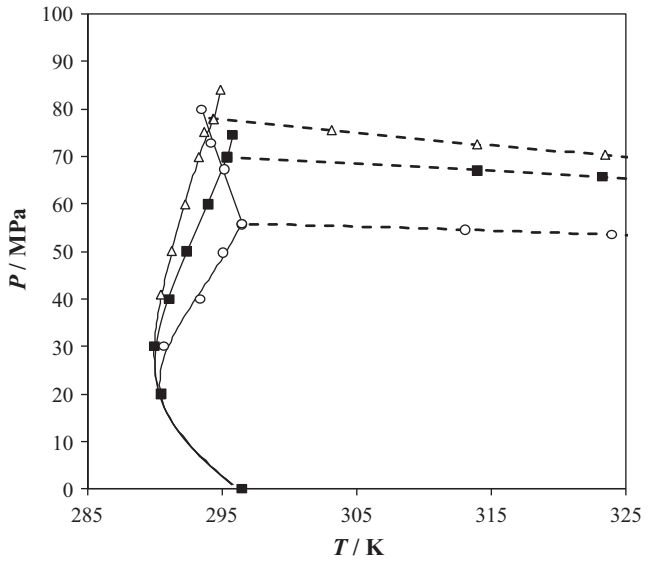

Fig. 3. *P*–*T* phase diagram of the system methane + waxy fraction for overall compositions (in mol% of CH_4) higher than 95%. Full line: wax disappearance temperatures; dotted line: dew pressures. △: 96% of methane; ■: 98% of methane; ◯: 99% of methane.

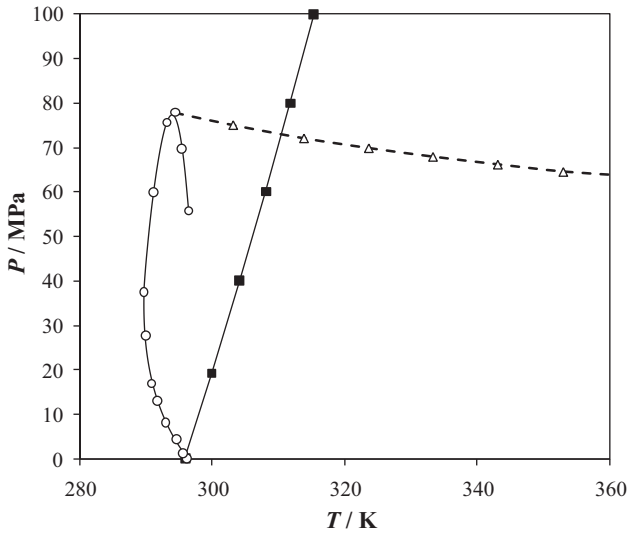

Fig. 4. *P–T* projection of the phase diagram in temperature range investigated. ○: crossover between liquid–vapor and fluid–solid phase transition lines; △: liquid–vapour critical curve; ■: wax disappearance temperature of the waxy fraction alone.

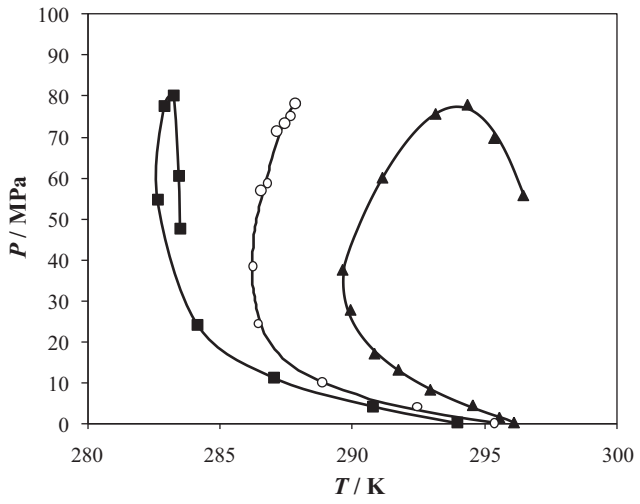

Fig. 5. *P–T* projection of crossover points. ▲: methane + waxy fraction; ■: methane + ternary waxy fraction [17]; ○: methane + pure heptadecane [16].

for the mixture having 99 mol% of methane. The phase boundaries between the (L + V + S) and (L + V) regions drastically change from one mixture to another and do not overlap in this composition domain. It can be observed that the pressure of the minimum in temperature decreases as the methane content increases. This behaviour is also linked to the presence of several paraffins into the mixture and becomes more pronounced in case of rich gas mixtures. In these systems, the heaviest paraffins are the first to crystallise [25,26] and consequently the wax starts to precipitate at higher temperatures.

Critical conditions were determined by performing several fluid phase equilibrium experiments between 90% and 96%. Experimentally, the mixture with 95.1% of methane came close to the critical conditions in the temperature range between 283 and 373 K. The fluid phase transitions of this mixture are displayed in Fig. 4 along with the projection of the crossover points between liquid–vapour and fluid–solid transition lines. The WDT of the waxy fraction was added to this figure. The projection of the crossover points for the multicompound mixture does not end when it intersects the liquid–vapour critical line at the upper critical endpoint whereas the L–V–S three phase equilibrium curve of real binary systems does. At this point the projection of the crossover point presents a maximum in pressure and the L–V critical curve is tangent to the crossover curve. This behaviour was previously observed in the system methane + (n-C_{16} + n-C_{17} + n-C_{18}) [17] but in this last case the effect is more significant. A comparison on the crossover line of both systems, as well as for the binary mixture (Fig. 5) reveals the strong influence of the distribution shape of the waxy fraction. The maximum pressure is almost the same (around 78 MPa). This value corresponds to the L–V critical line that depends more on the molecular weight of the heavy fraction than on its composition. On the opposite the minimum temperature is affected by the n-paraffin distributions. It appears at higher temperature for the long paraffin distributions than for the ternary waxy fraction. The curve of the real binary system appears at intermediate temperatures between the two pseudo-binary systems. This behaviour which was previously observed for the melting temperature of the neat waxy fraction is exacerbated by the addition of methane. At the maximum pressure a difference of more than 10 K is observed between the two pseudo-binaries. This observation shows the large importance of the concentrations of the heavy components of the waxy fraction on the liquid–solid phase equilibrium and above all on the vapour–solid phase equilibrium. It thus plays a major role on the wax deposition from condensate gases.

From the full set of isopleth data, *P–x* diagrams can be drawn at fixed temperatures. However as the phase transition measurements were not carried at identical temperatures for all the mixtures, these curves cannot be directly plotted from the original data but need to be interpolated from the experimental values. This was done by performing low-degree polynomial fits of the experimental data. The results are plotted in Fig. 6 for the isotherms 300, 330 and 360 K. The values measured in the binary system C_1 + n-C_{17} [16] as well as in the pseudo binary C_1 + (n-C_{16} + n-C_{17} + n-C_{18}) [17] are also displayed in this diagram. It can be seen that in the vicinity of the critical condition the pseudo binary with a long distribution presents a transition pressure 2 MPa higher than those for the other systems. This critical pressure increase comes from the presence of the heavier components in the waxy fraction. Apart from the critical neighborhood, the three sets of data behave similarly. Thus, the waxy distribution can be assumed as a single pseudo-paraffin with a molecular weight equal to the average molecular weight

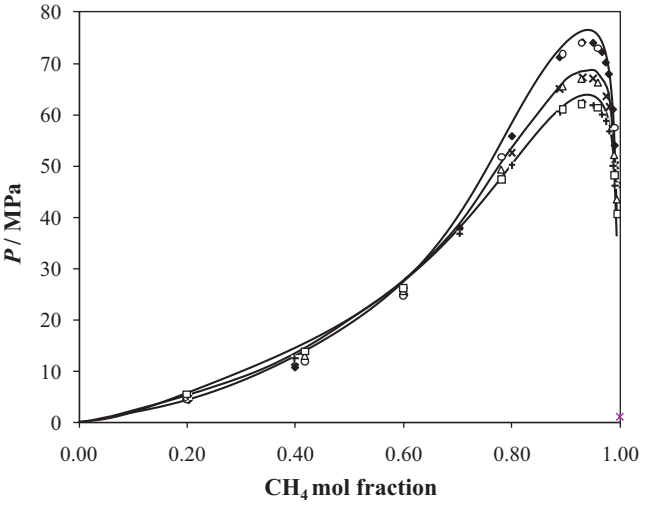

Fig. 6. *P–x* phase diagram. Hollow symbols: methane + ternary waxy fraction [16] (○: 300 K; △: 330 K; □ 360 K). Cross symbols: methane + pure heptadecane [16] (♦: 300 K; ×: 330 K; +360 K). Lines: methane + waxy fraction at *T* = 300, 330 and 360 K.

of the heavy fraction when considering only liquid–vapour phase equilibrium.

4. Conclusion

The phase diagram of a pseudo binary system made up of a methane + a regular distribution of normal paraffins ranging from n-C_{13} to n-C_{22} and having an average molecular weight equal to heptadecane was experimentally investigated by measuring both liquid–vapour and fluid–solid phase transitions. Comparisons of results with previous measurements performed on the binary system C_1 + n-C_{17} [16] and on the pseudo binary C_1 + (n-C_{16} + n-C_{17} + n-C_{18}) [17] confirm that the regular waxy fraction can be considered as a single pseudo component having the same molecular weight for liquid–vapour phase equilibrium calculation but not for fluid–solid phase equilibria. The shape and the size of the paraffin distribution play an important role on wax appearance temperatures as well as on the influence of gas on vapour–solid phase transition. Consequently, the calculation of wax precipitation from gas condensates requires a thermodynamic model that takes into account a detailed description of the paraffin distribution.

References

[1] P. Ungerer, B. Faissat, C. Leibovici, H. Zhou, E. Behar, G. Moracchini, J.P. Courcy, Fluid Phase Equilibr. 111 (1995) 287–331.
[2] M.R. Jensen, P. Ungerer, B. de Weert, E. Behar, Fluid Phase Equilibr. 208 (2003) 247–260.
[3] J.L. Daridon, J. Pauy, J.A.P. Coutinho, F. Montel, Energy Fuels 15 (2001) 730–735.
[4] H. Pan, A. Firoozabadi, P. Fotland, SPE Production & Facilities, November, 1993, pp. 250–258.
[5] V. Ruffier Meray, J.L. Volle, C.J.P. Schranz, P. Le Marechal, E. Behar, SPE 26549 (1993) 369–373.
[6] T.S. Brown, V.G. Niesen, D.D. Erickson, SPE 28505 (1994) 415–430.
[7] J. Pauly, J.L. Daridon, J.A.P. Coutinho, Fluid Phase Equilibr. 187–188 (2001) 71–82.
[8] E. Flöter, Th.W. de Loos, J. de Swaan Arons, Int. J. Thermophys. 16 (1995) 185–194.
[9] E. Flöter, Th.W. de Loos, J. de Swaan Arons, Fluid Phase Equilibr. 117 (1996) 153–159.
[10] E. Flöter, Th.W. de Loos, J. de Swaan Arons, Fluid Phase Equilibr. 127 (1997) 129–146.
[11] E. Flöter, C. Brumm, Th.W. de Loos, J. de Swaan Arons, J. Chem. Eng. Data 42 (1997) 64–68.
[12] E. Flöter, P. van der Pijl, Th.W. de Loos, J. de Swaan Arons, Fluid Phase Equilibr. 134 (1997) 1–19.
[13] E. Flöter, B. Hollanders, Th.W. de Loos, J. de Swaan Arons, Fluid Phase Equilibr. 143 (1998) 185–203.
[14] J.J.B. Machado, Th.W. de Loos, Fluid Phase Equilibr. 222–223 (2004) 261–267.
[15] J.J.B. Machado, Th.W. de Loos, Fluid Phase Equilibr. 226 (2004) 83–90.
[16] J. Pauly, J.A.P. Coutinho, J.L. Daridon, Fluid Phase Equilibr. 255 (2007) 193–199.
[17] J. Pauly, J.A.P. Coutinho, J.L. Daridon, Fluid Phase Equilibr. 297 (2010) 149–153.
[18] H.J. van der Kooi, E. Flöter, Th.W. de Loos, J. Chem. Thermodyn. 27 (1995) 847–861.
[19] J.-L. Daridon, J. Pauly, M. Milhet, Phys. Chem. Chem. Phys. 4 (2002) 4458–4461.
[20] J. Pauly, J.L. Daridon, J.A.P. Coutinho, N. Lindeloff, S.I. Andersen, Fluid Phase Equilibr. 167 (2000) 145–159.
[21] J.M. Sansot, J.M.J. Pauly, J.L. Daridon, J.A.P. Coutinho, AIChE J. 51 (2005) 2089–2097.
[22] U.K. Deiters, S.L. Randzio, Fluid Phase Equilibr. 260 (2007) 87–97.
[23] M. Glaser, C.J. Peters, H.J. Van Der Kooi, J. Chem. Thermodyn. 17 (1985) 803–815.
[24] S.L. Randzio, Ch. Stachowiak, J.P.E. Grolier, J. Chem. Thermodyn. 35 (2003) 639–648.
[25] A.J. Briard, M. Bouroukba, D. Petitjean, N. Hubert, J.C. Moise, M. Dirand, Fuel 84 (2005) 1066–1073.
[26] A.J. Briard, M. Bouroukba, D. Petitjean, N. Hubert, J.C. Moise, M. Dirand, Fuel 85 (2006) 764–777.